Plate–concrete interfacial bond strength of FRP and metallic plated concrete specimens

S.K. Sharma[a,*], M.S. Mohamed Ali[a], D. Goldar[b], P.K. Sikdar[c]

[a]*Bridges area, Central Road Research Institute, New Delhi 110-020, India*
[b]*Department of Civil Engineering, Delhi College of Engineering, University of Delhi 110-007, India*
[c]*Department of Civil Engineering, IIT Bombay, Powai 400076, India*

Abstract

Bonding of steel or fibre reinforced polymer (FRP) plates by adhesive to the surface of concrete structural elements have become increasingly popular for improving their strength and stiffness. However, these plates are susceptible to debonding prematurely before reaching the designed strength. Therefore, a thorough knowledge of bond behaviour of concrete–adhesive–plate interface is a prerequisite to develop guidelines to avoid failure through the different possible modes. The paper presents thirty six (36) test results for single shear tests conducted on concrete prisms bonded with variety of FRP and metallic plates to evaluate the bond strength and the critical bond length required to sustain the maximum stress on bond for a given plate–concrete interface. The elastic modulus and ultimate tensile strength of the plates of different materials vary between 32–300 GPa and 196–2800 MPa respectively. The design guidelines developed in this study are capable of predicting the critical bond length and ultimate bond strength of any type of plate–concrete interface with good accuracy. The predictability of the ultimate bond strength model is validated using numerous test results taken from the published literature.
© 2005 Elsevier Ltd. All rights reserved.

Keywords: Critical bond length

1. Introduction

Rehabilitating and retrofitting of existing civil engineering infrastructures have become a common necessity since the past two decades. It has become an even more significant need to upgrade and repair the existing ageing structures rather than building new ones. In a developing country like India, some one thousand major bridges on the National Highway system need rehabilitation at a whopping cost of Rupees 10 billion (US$ 200 million). Therefore, inexpensive and unobtrusive rehabilitation technique such as adhesive bonding of steel or FRP (fibre reinforced polymer) plates to the surfaces of reinforced concrete structures may be very useful opinion. Steel plates were used in the early applications of the method, but the plates of fibre reinforced polymer (FRP) material are now being used more frequently due to their superior strength and other enhanced properties.

The failure behaviour of the plate is dictated by the integrity of the plate with the original concrete member through adhesive bonding, which plays the role of a shear connector between the plate and the original RC member. However, these bonded plates are prone to many failure mechanisms as categorized [1]. Therefore, an important issue in the design of effective retrofitting solution using externally bonded plates is the bond strength. The paper is concerned with the bond strength and the critical bond length, which is defined as the length of the externally bonded plate, beyond which there is no further increase in the axial load carrying capacity of the plate–adhesive–concrete interface. To understand the failure/debonding mechanism of the plates, complete knowledge of the bond behaviour of the plate–adhesive–concrete interface is a prerequisite [2].

There is plenty of experimental data available on the behaviour of FRP plated concrete beams under the axial load i.e. single or double shear test [3–15]. However, no unique design procedure is available for the determination of the concrete–adhesive–plate interfacial bond strength

* Corresponding author. Tel.:+91 11 2631 4424; fax: +91 11 2684 5943, 2683 0480.
E-mail address: sksharma@crridom.org (S.K. Sharma).

Notation

Al	aluminium
b_c	width of concrete prism
b_p	width of the bonded plate
CFRP	carbon fibre reinforced polymer
d_b	depth of concrete prism
E_c	Young's modulus of concrete
E_p	Young's modulus of plate
P	current applied load
f_b	Brazilian or splitting tensile strength of concrete
f_c	cylinder compressive strength of concrete
P_u	ultimate debonding/fracture load
f_p	tensile strength of plate
GFRP	glass fibre-reinforced polymer
K	constant
L_b	bond length of plate
$L_{b,crit}$	critical bond length
L_t	length of transverse stress distribution
P_b	bond strength of bonded plate
$P_{i,cr}$	initial cracking load
S	steel
t_p	thickness of the bonded plate
β_p	width factor
τ	shear stress
τ_{av}	average shear stress
τ_{pk}	peak shear stress

(P_b) and critical bond length ($L_{b,crit}$) for metallic and FRP bonded plates [6,9]. The bond failure is largely due to crack propagation near or along the adhesive-concrete interface parallel to the length of the plate. The crack initiates in the vicinity of the most stressed end and propagate further towards the free end of the plate, and the debonding in such case is defined as shear debonding failure. It is one of the major types of failure modes in the beams or slabs strengthened with plate/strip for flexural capacity [16,17].

Peak shear strength is a function of tensile strength of concrete [3,6,10]. Thickness of the adhesive has negligible effect on mean and peak shear stresses [4,14,18]. Stress concentrations at the end of the plate are another cause of premature bond failure for beams strengthened for flexure capacity [4,19–24]. Plate–adhesive–concrete interfacial bond strength is reported to range between 1.5 and 15 MPa [25]. The effects of various parameters, such as the anchorage length, glue thickness and the strength of the concrete, on bond strength of the plated specimens have also been studied by many researchers [3,6,26,27]. Most of the studies are limited in nature as these have considered only a few parameters such as constant bond length, thin plate (0.11–0.22 mm), and adhesive type that affect the axial peeling [2]. An exhaustive review on the anchorage behaviour of single/double shear tests along with the practical engineering models has been presented [27].

The present study aims to provide an understanding of the bond behaviour at the plate–adhesive–concrete interface with different types of metallic and FRP plates. Thirty-six tests were conducted on concrete prisms using metallic and FRP plates with elastic modulus ranging from 32 to 300 GPa, having ultimate tensile strength ranging between 196 to 2800 MPa and keeping bond lengths between 50 and 300 mm. It is necessary to develop simple design guidelines to determine the ultimate bond strength (P_b) across plate–adhesive–concrete interface as well as the critical bond length ($L_{b,crit}$) for any type of plate, and to calibrate the developed model with the test results obtained from published research (based on the failure mode that occurred in the concrete a few mm beneath the concrete–adhesive interface).

2. Specimen properties and experimental setup

2.1. Material properties

Thirty six concrete prisms measuring 100 mm × 100 mm × 500 mm were fabricated consisting a concrete mix by mass with the ratio: 1.0 (ordinary Portland cement): 1.3 (sand): 3.5 (coarse aggregate of 10 mm maximum size), and a water-cement ratio 0.40. The cylinder compressive strength of concrete (f_c), Brazilian or splitting tensile strength of concrete (f_b) and elastic modulus of concrete (E_c) (size of cylinder 150 mm diameter and 300 mm length) were determined in the laboratory on the same day on which the testing of the plated prisms was done. The average cylinder compressive strength f_c, splitting tensile strength of concrete f_b and elastic modulus of concrete E_c are given in Table 1. Plates of six different categories, i.e., glass fibre reinforced polymer (GFRP) with an elastic modulus (E_p) of 32.7 GPa, aluminium (Al) with $E_p = 74.85$ GPa, steel (S) of $E_p = 208$ GPa and three types of carbon fibre reinforced polymer (CFRP) plates with elastic moduli 165, 210 and 300 GPa were used in the study. The ultimate tensile strength (f_p) of the plates used in the study are shown in Table 1. The epoxy resin used for bonding the plates had a compressive and tensile strengths of 80 and 17.8 MPa.

2.2. Test setup

The concrete surface of the prism was roughened using a mechanical grinder to remove the surface laitance and expose the coarse aggregates. Dust and any loose particles were blown off by means of compressed air. The surface of the FRP plate was also roughened with emery paper to take

Table 1
Material properties

Specimen	Concrete			Plate	
	Comp. strength, f_c (MPa)	Young's modulus, E_c (GPa)	Tensile strength, f_b (MPa)	Young's modulus, E_p (GPa)	Tensile strength, f_p (MPa)
GFRP-32.7	35.82	35.3	3.08	32.7	384
Aluminum-74.8	34.6	31.9	3.46	74.8	196
Steel-208	35.82	35.3	3.08	208	565
CFRP-165	29.7	36.4	3.44	165	2800
CFRP 210	35.82	35.3	3.08	210	2400
CFRP-300	29.7	36.4	3.44	300	1300

the surface shine off the plate without any damage to fibre or its orientation at the surface level. In the case of metallic plates, the surface was grit blasted to remove mill scale and grease and cleaned with acetone before bonding to the concrete. The plate of required bond length was bonded on the surface of the prism and the length of the bonded joint was designated as bond length L_b (Fig. 1). The plates were clamped in position on the test specimens for ten days to bond the plate and allow the epoxy adhesive to harden sufficiently. Electrical resistance strain gauges (120-Ohm) were fixed on the plate at different locations as shown in Fig. 1. After the required curing, the specimen was housed in a steel test frame (Fig. 2) similar to the one used by others [12]. The test assembly was held in plumb line so that there would be a direct shear at the plate–concrete interface. The top surface of the concrete specimen came in contact with the top bearing plate of the frame and the extended part of the bonded plate was held in the top grips. The bottom plate of the frame was held in the bottom grips of the machine. The concrete specimens were secured inside the steel frame. An axial tensile force was applied to the plate through the machine and the strain magnitudes at various locations along the joint in the bonded plate at different stages of the applied load were recorded with a strain indicator. The shear debonding mode of plate–concrete interface was observed for all the test specimens.

In the present study, tests in six different series were conducted and they are designated as GFRP-32.7, Aluminium-74.8, Steel-208, CFRP-165, CFRP-210 and CFRP-300. Bond lengths ranging between 50 and 300 mm were considered in the study (Table 2). The specimens were labeled with alphanumeric designation depending upon the type of the plate, modulus of elasticity and bonded length. The number following the type of material represents the modulus of elasticity and the number after the hyphen is the bonded length of the plate.

3. Test results

The complete test matrix is listed in Table 2. The strain variation along the bonded joint (strains were measured on the plate surface, not at plate–concrete interface) at various load levels, and the shear stress as a function of load level was determined for all the tests. The crack propagation was monitored visually. The test results of only specimen G32.7-100 for the series GFRP-32.7 is discussed in detail, while the significant observations from other test series are summarised.

3.1. GFRP-32.7 series

3.1.1. Crack growth and debonding mode

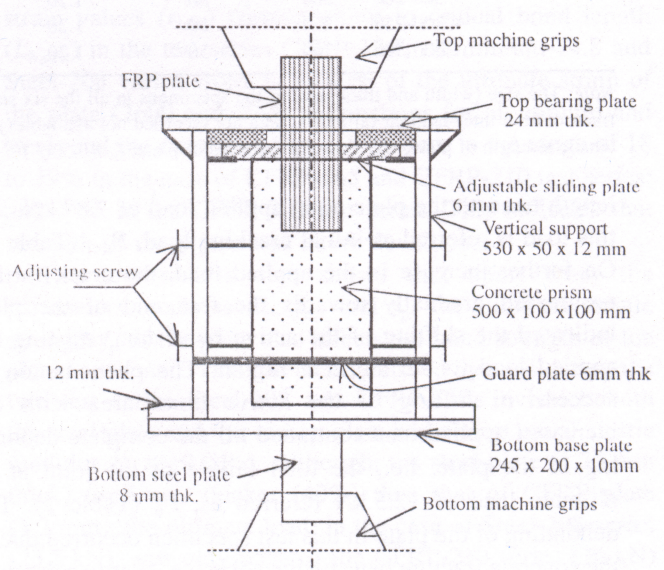On applying axial load to the plate, a crack of length 20 mm occurred at the most stressed end along the plate
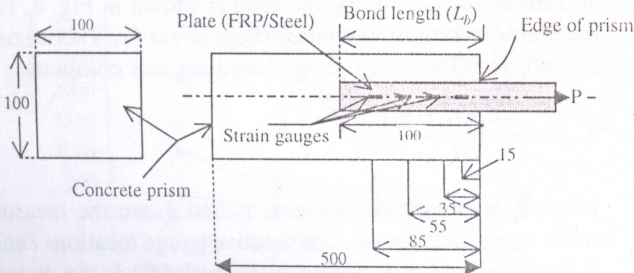

Fig. 1. Specimen for single shear test.

Fig. 2. Schematic diagram of steel test frame.

Table 2
Results from present tests

Test series	Specimen reference no.	Bond length, L_b (mm)	Width of plate, b_p (mm)	Thickness of plate, t_p (mm)	Measured strain (10^{-6})	Initial cracking load (kN)	Measured ultimate failure load, P_u (kN)	Axial tensile capacity of plate, $f_p A_p$ (kN)	Theoretical load, P_b, Eq. (11a) and (11b) (kN)	Failure mode
GFRP-32.7	G32.7-100	100	30	4.00	4080	7.87	12.50	46.00	10.79	CF
	G32.7-150	150	30	4.00	4770	12.12	17.74	46.00	16.18	CF
	G32.7-175	175	30	4.00	5050	5.12	20.50	46.00	18.87	CF
	G32.7-200	200	30	4.0.0	4340	18.00	20.60	46.00	20.24	CF
	G32.7-250	250	30	4.00	7135	18.10	20.40	46.00	20.24	CF
	G32.7-300	300	30	4.00	6535	14.98	20.30	46.00	20.24	CF
Aluminium-74.8	Al74.8-150	150	30	6.00	1370	12.00	19.44	35.28	16.14	CF
	A74.8-200	200	30	6.00	1025	10.12	25.14	35.28	22.59	CF
	Al74.8-250	250	30	6.00	1120	17.50	24.90	35.28	26.89	CF
	Al74.8-280	280	30	6.00	1730	10.00	26.02	35.28	27.67	CF
	A74.8-300	300	30	6.00	*	*	25.40	35.28	27.67	CF
Steel-208	S208-50	50	50	1.72	*	*	11.30	48.60	9.83	CF
	S208-75	75	50	1.72	*	*	16.25	48.60	17.52	CF
	S208-100	100	50	1.72	730	12.78	22.12	48.60	21.90	CF
	S208-125	125	50	1.72	*	*	21.25	48.60	25.63	CF
	S208-150	150	50	1.72	1580	15.10	22.80	48.60	25.63	CF
	S208-200	200	50	1.72	1475	17.54	23.50	48.60	25.63	CF
	S208-255	255	50	1.72	1350	17.50	22.90	48.60	25.63	CF
CFRP-C165	C165-100	100	50	1.20	1530	14.40	18.25	168.00	21.25	CF
	C165-130	130	50	1.20	*	*	24.50	168.00	27.25	CF
	C165-150	150	50	1.20	3425	15.08	28.44	168.00	31.87	CF
	C165-175	175	50	1.20	2900	20.32	32.00	168.00	34.23	CF
	C165-200	200	50	1.20	3160	27.46	34.22	168.00	34.23	CF
	C165-250	250	50	1.20	2825	20.36	33.14	168.00	34.23	CF
	C165-300	300	50	1.20	3150	26.00	34.24	168.00	34.23	CF
CFRP-C210	C210-150	150	50	1.20	*	*	30.40	144.00	26.93	C F&FF
	C210-180	180	50	1.20	2265	27.80	34.00	144.00	32.30	C F&FF
	C210-190	190	50	1.20	*	*	36.00	144.00	35.90	C F&FF
	C210-200	200	50	1.20	2040	30.12	36.02	144.00	36.03	C F&FF
	C210-230	230	50	1.20	1750	32.00	37.02	144.00	36.03	C F&FF
	C210-255	255	50	1.20	2250	30.10	36.80	144.00	36.03	C F&FF
CFRP-C300	C300-160	160	50	1.20	1000	10.00	38.02	78.00	34.31	C F&FF
	C300-180	180	50	1.20	920	25.24	41.15	78.00	38.60	C F&FF
	C300-200	200	50	1.20	1920	24.80	46.35	78.00	40.96	C F&FF
	C300-250	250	50	1.20	1880	20.16	45.50	78.00	40.96	C F&FF
	C300-300	300	50	1.20	1345	17.54	45.95	78.00	40.96	C F&FF

Note: The size (width and thickness) of the specimens in all the six series is 100 mm×100 mm. CF, concrete fracture; CF&FF, concrete fracture and fibre fracture/fibre inter-laminar failure; *, data not recorded/not available; f_c, cylindrical compressive strength of concrete; E_c, Young's modulus of concrete; f_p, tensile strength of plate; E_p, Young's modulus of plate; $f_b = 0.53(f_c)^{0.5}$ (ACI 318-89) [31].

length beneath the plate at an applied load of 7.87 kN, and this load is referred as initial cracking load, $P_{i,cr}$ (Table 2). On further increase in the applied load, the crack further progressed gradually towards the free end of the plate indicated the shifting of the active bond area resisting the applied load to the adjacent region. The phenomenon of successive shifting of the active bond area with the increased applied load continued till the complete debonding of the plate, i.e., the total failure of the joint at an ultimate load of 12.5 kN referred as, P_u (Table 2). The debonding of the plate in this test specimen occurred due to the concrete fracture beneath the adhesive layer to a depth of about 10–15 mm in the vicinity of the most stressed end, which gradually reduced to 2–3 mm at the free end of the plate (i.e. end of fracture zone) as shown in Fig. 3(a).

3.1.2. Axial strain and shear stress distribution

The variation in the measured strain at different gauge locations along the bond length for the specimen G32.7-100 at different stages of applied load is shown in Fig. 4. From the measured strain, the mean shear stress (τ_{i-j}) between the two consecutive strain gauge locations was computed.

$$\tau_{i-j} = \frac{t_p E_p (g_i - g_j)}{\Delta l_{i-j}} \tag{1}$$

where t_p is the plate thickness, g_i and g_j are the measured strain magnitudes at two consecutive gauge locations i and j, E_p is the elastic modulus of plate, and Δl_{i-j} is the distance between the two gauge locations. Using Eq. (1), the shear stress along the joint for the specimen G32.7-100 was calculated and is shown in Fig. 4 as a function of applied
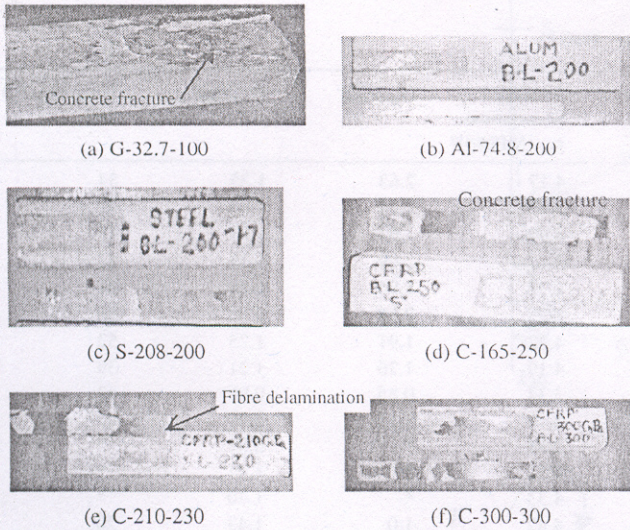
(a) G-32.7-100   (b) Al-74.8-200

(c) S-208-200   (d) C-165-250

(e) C-210-230   (f) C-300-300

Fig. 3. Typical failure mode of plated specimens.

load. The load in this plot is normalized by the maximum applied load before plate separation, P_u. It can be seen that the shear stress between the two gauge locations next to the loaded end of the plate, indicated by 15–35 mm, reached a peak value at a normalised load of 0.63 and then decreased abruptly. The abrupt decrease indicated the initiation of plate debonding and the corresponding load referred as initial cracking load $P_{i,cr}$. The initial plate separation occurred at 17% of the axial tensile capacity of plate as listed in Table 3. After initial separation the average shear stress at other sections along the plate increased indicating a shift of the active bond area to this region (Fig. 5).

The magnitude of the maximum measured axial strain, ε_{test}, in the plate along the joint (G32.7-100) was 4080 microstrain corresponding to an applied load of 11.75 kN (Fig. 4). This was about 34% of the ultimate strain of GFRP plate (Table 3), determined from the ratio with f_p/E_p (11,750 micro strain).

The critical bond length ($L_{b,crit}$) for this series (GFRP-32.7) of tests was 175 mm, which corresponds to an ultimate load, P_u, equal to 20.5 kN, beyond which there was no
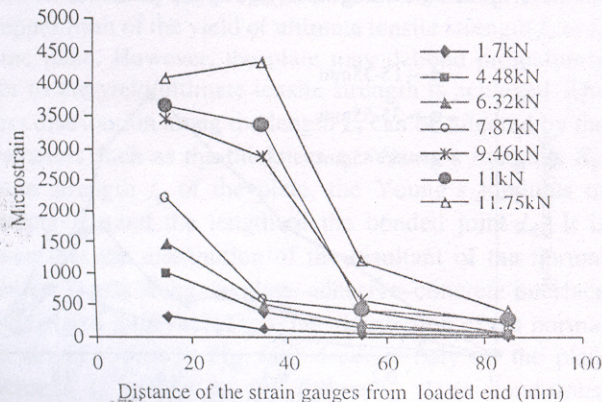
appreciable variation in the ultimate load (Table 2). The ultimate failure load (P_u) for the specimen G32.7-100 was 27% of the axial tensile capacity of the plate (Table 3).

The ratio of the peak shear stress (τ_{pk}), defined as the maximum value of shear stress corresponding to initial concrete cracking load ($P_{i,cr}$) to the splitting tensile strength (f_b) of concrete of the specimen, was 2.63. For specimen G32.7-100 the average shear stress (τ_{av}), defined as the ratio of the ultimate load (P_u) to the bonded area ($L_b b_p$) along the joint, was 1.35 times the splitting tensile strength, f_b (or f_t). The ratios are given for all the tests in Table 3.

4. Significant observations from other test series

The results from all the test series are summarized in Table 3 and the significant observations are briefly discussed here. In all the tests, once the debonding crack initiated in the neighborhood of most stressed region, the active area got shifted towards the free end of the plate. This phenomenon kept recurring till the complete debonding of the plate occurred. The plates mainly debonded due to the concrete fracture (CF) under the adhesive layer except in the case of the test series CFRP-210 and CFRP-300, where the mode of debonding was a combination of concrete fracture and fibre delamination (Fig. 3(b–f). The measured failure loads (P_u) corresponding to critical bond length ($L_{b,crit}$) in the series Aluminium-74.8 and Steel-208 were 71 and 48% of the axial tensile capacity of the plates and the corresponding values in the case of GFRP-32.7 test series was 45%. In the case of the prisms bonded with carbon FRP plates (test series; CFRP-165, CFRP-210 and CFRP-300), the magnitude of measured failure loads (P_u) corresponding to $L_{b,crit}$ were about 20, 26 and 59% of the strength of the plates, respectively. The magnitude of the maximum measured strain values (ε_{test}) corresponding to critical bond length ($L_{b,crit}$) in the test series GFRP-32.7, Aluminium-74.8 and Steel-208 varied from 37 to 40% of the ultimate strain of the plate (2600 and 2700 microstrains for aluminium and steel) and the corresponding values were in the range of 18 to 19% in the case of CFRP-165 and CFRP-210 test series; and 44% in the CFRP-300 test series. This indicates that strength of the plates was never developed.

The test results also shows that apart from the parameters, such as E_p, f_b, and t_p, the ultimate tensile strength f_p of the plate also affects the bond strength of the plated specimen. This can be established by considering the two test series Steel-208 and CFRP-210, in which both the steel plate and the carbon plate had almost equal elastic modulus E_p (210 GPa). Although, the steel plate (1.72 mm thick) used was thicker (40%) than that of CFRP plate (1.2 mm), the ultimate load, in the case of Steel-208 series (23.5 kN), was only 65% of the CFRP-210 series (36 kN) (Table 2). This is due to the fact that the ultimate tensile strength of the CFRP-210 plate (2400 MPa) was more than

Fig. 4. Strain measurement along the joint (G32.7-100).

Table 3
Summary of test results

Test series	Specimen reference no.	$\{P_{i,cr}/f_pA_p\} \times 100$	$\{P_u/f_pA_p\} \times 100$	Peak shear stress, τ_{pk} (MPa)	Average Shear stress, τ_{av} (MPa)	$(\tau_{pk})/(f_b)$	$(\tau_{av})/(f_b)$	$\{(\epsilon_{test})/(f_p/E_p)\} \times 100$
GFRP-32.7	G32.7-100	17	27	8.10	4.17	2.63	1.35	34
($L_{b,crit}$ =	G32.7-150	26	38	7.82	3.94	2.54	1.28	41
175 mm)	G-32.7-175	11	44	5.14	3.90	1.67	1.27	43
	G32.7-200	39	45	6.45	3.43	2.09	1.11	37
	G32.7-250	39	44	6.04	2.72	1.96	0.88	61
	G32.7-300	32	44	8.26	2.25	2.68	0.73	56
Aluminium-	A174.8-150	34	55	6.62	4.32	1.91	1.25	52
74.8 ($L_{b,crit}$ =	A174.8-200	29	71	4.37	4.19	1.26	1.21	39
200 mm)	A174.8-250	50	70	2.95	3.32	0.85	0.96	43
	A174.8-280	28	73	3.92	3.10	1.13	0.90	66
	A174.8-300	*	71	*	2.82	*	0.81	*
Steel-208	S208-50	*	23	*	4.52	*	1.47	*
($L_{b,crit}$ =	S208-75	*	33	*	4.33	*	1.40	*
200 mm)	S208-100	26	45	3.09	4.42	1.0	1.43	20
	S208-125	*	44	*	3.40	*	1.10	*
	S208-150	31	47	6.39	3.04	2.07	0.99	43
	S208-200	36	48	6.27	2.35	2.03	0.76	40
	S208-255	36	47	3.52	1.80	1.14	0.58	37
CFRP-C165	C165-100	08	11	8.49	3.65	2.47	1.06	09
($L_{b,crit}$ =	C165-130	*	15	*	3.77	*	1.09	*
200 mm)	C165-150	09	17	7.95	3.79	2.31	1.10	20
	C165-175	12	19	6.51	3.70	1.89	1.07	17
	C165-200	16	20	5.22	3.42	1.52	0.99	19
	C165-250	12	19	5.52	2.65	1.60	0.77	17
	C165-300	15	20	5.78	2.28	1.68	0.66	18
CFRP-C210	C210-150	*	21	*	4.05	*	1.31	*
($L_{b,crit}$ =	C210-180	19	24	5.89	3.78	1.75	1.23	20
230 mm)	C210-190	*	25	*	3.80	*	1.23	*
	C210-200	21	25	6.88	3.60	2.23	1.25	18
	C210-230	22	26	8.25	3.22	2.68	1.04	15
	C210-255	21	25	9.52	2.88	3.09	0.93	20
CFRP-C300	C300-160	13	49	3.77	4.75	1.09	1.38	23
($L_{b,crit}$ =	C300-180	32	53	4.58	4.57	1.33	1.33	21
200 mm)	C300-200	32	59	9.24	4.63	2.68	1.34	44
	C300-250	26	58	4.07	3.64	1.18	1.06	43
	C300-300	22	59	4.75	3.06	1.38	0.89	31

Note: *, data not recorded.

the Steel-208 plate (565 MPa) which leads to an important conclusion that the tensile strength (f_p) of the plate has an impact on the bond strength (P_b). Furthermore, the ratios of the peak shear stress along the joint to the splitting tensile strength of concrete (τ_{pk}/f_b) corresponding to the critical bond length ($L_{b,crit}$) of all the tests conducted in the present study ranged between 1.26 and 2.68 (Table 3).

5. Analysis of test results

The plate–concrete interface bond strength is similar to that of the bond between the steel reinforcement and the concrete like a normal reinforced concrete structure (bond between the reinforcement and the surrounding concrete). Apart from the properties of the concrete and of the reinforcement, the bond behaviour between the rebar and the concrete depends upon the development length, which is

required to carry and to transfer the load to the surrounding concrete. Similar is the case with the plated beam, where the plate–concrete interface bond strength, P_b, also depend on the critical bond length, $L_{b,crit}$, of the plate.
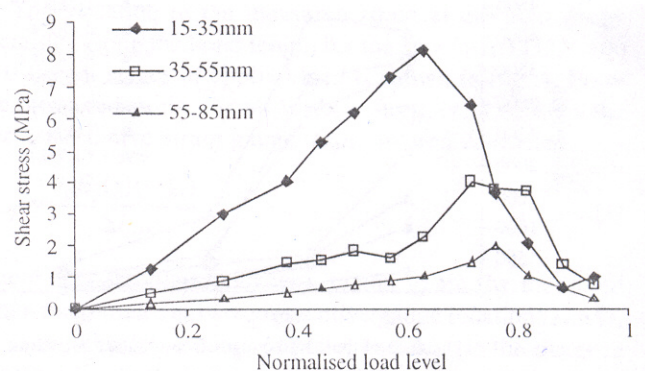

Fig. 5. Shear stress distribution for GFRP plate (G32.7-100).
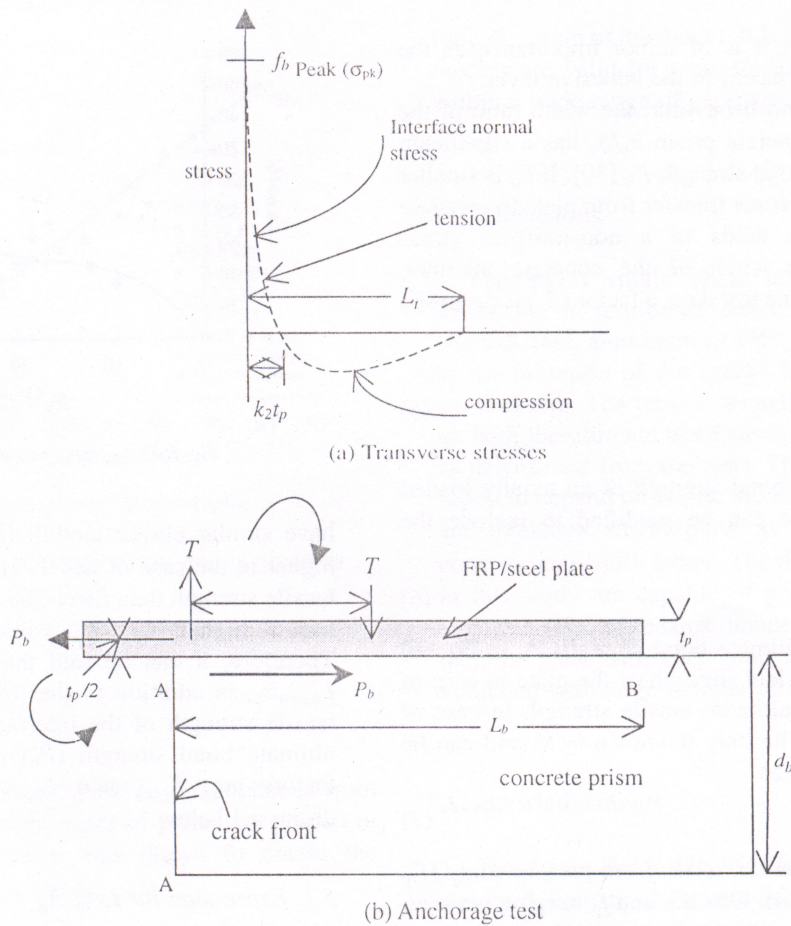
(a) Transverse stresses

(b) Anchorage test

Fig. 6. Distribution of normal stresses along the bonded joint (Oehlers and Moran 1990, Ali et al.2000).

The stress distributions for both the longitudinal shear and normal peeling stresses were derived from classical analysis provided [20] and computer simulations [21]. The normal stress in the plate–adhesive–concrete interface has distribution as shown in Fig. 6(a). The maximum tensile stress occurs at the loaded end of the plate (edge A–A of the bond area), leading to the debonding of the plate. From the extensive tests on concrete prisms (present study) and as reported in literature [9], the failure occurred by the cracking and splitting in the concrete, the maximum tensile stress assumed, to be f_b. The axial force P_b in Fig. 6(b) has an upper limit of the yield or ultimate tensile strength f_y or f_p of the plate. However, the plate may debond prematurely prior to the yield/ultimate tensile strength is achieved. The stress distribution along the length L_t can be affected by the parameters such as the thickness t_p, Young's modulus E_p, tensile strength f_p of the plate, the Young's modulus of concrete E_c, and the length of the bonded joint L_b. It is shown that the distribution of the resultant of the normal stresses, T, acts along the plate–adhesive–concrete interface of the plated joint [21]. Thus, the distribution of the normal stresses as shown in Fig. 6(a) depends only on the plate thickness t_p subject to the following three conditions. Firstly, the material stiffness of the plate and that of

the concrete prism should remain constant. Secondly, the plate thickness t_p should be much less than that of the prism and this occurs normally in practice. Finally, the length of the bonded plate L_b should be greater than the length of the transverse stress distribution L_t as shown in Fig. 6(a). Axial loading on the plate induces the force T normal to the prism surface and from the equilibrium of the forces in Fig. 6(b) the equation for P_b can be written as

$$P_b t_p = 2Tk_1 t_p \qquad (2)$$

If the mean tensile stress $s_a f_b$ acts in the tensile region of length $k_2 t_p$ in Fig. 6(a), then the resultant normal force T becomes

$$T = s_a k_2 t_p b_p f_b, \qquad (3)$$

where s_a can be visualized as a shape factor of constant magnitude, i.e. the ratio of the mean-to-maximum tensile peeling stress in the region L_t. Now on substitution, Eq. (2) for the ultimate bond strength can be written as

$$P_b = K t_p b_p f_b, \qquad (4)$$

where $K = 2k_1 k_2 s_a$ and the coefficients k_1 and k_2 are constants. Though, the adhesive thickness affect the stress

distribution [28,29] but it is of minor importance as the failure did not occur adjacent to the adhesive layer.

Due to localized bond behaviour, the width ratio of the bonded plate to the concrete prism b_p/b_c has a significant effect on the ultimate bond strength P_b [30]. If b_p is smaller than that of b_c, then the force transfer from plate to concrete through the interface leads to a non-uniform stress distribution across the width of the concrete member. From the regression of the test data, a factor (β_p) is proposed [30] as

$$\beta_p = \sqrt{\frac{2 - (b_p/b_c)}{1 + (b_p/b_c)}} \tag{5}$$

Eq. (4) for ultimate bond strength of an axially loaded plate–concrete interface can be modified to include the width factor as

$$P_b = K\beta_p d_b t_p f_b \tag{6}$$

The magnitude of ultimate bond strength P_b in Eq. (6) should not exceed the yield strength of the plate in case of metallic plate and the ultimate tensile strength in case of FRP plate. In Eq. (6), the only unknown is K, and can be deduced by rearranging as

$$K = P_b/\beta_p b_p t_p f_b \tag{7}$$

The test results of the six series from present study (E_p ranging between 32.7 and 300 GPa and f_p ranging between 196.3 and 2800 MPa) and those reported [6] were used to develop a relationship between the ratio of L_b to t_p and K as shown in Fig. 7. It can be idealized from Fig. 7 that, the value of K increases linearly up to a critical value of $L_{b,crit}/t_p$, and thereafter the values of K remains constant at a magnitude of K_{crit} for the increased magnitudes of L_b/t_p, where K_{crit} is the maximum attainable value within the ascending branch of the curve of K and K can be written as

$$K = \frac{K_{crit}}{L_{b,crit}/t_p}\left(\frac{L_b}{t_p}\right), \quad \text{if } L_b/t_p < L_{b,crit}/t_p \tag{8a}$$

$$K = K_{crit}, \quad \text{if } L_b/t_p > L_{b,crit}/t_p \tag{8b}$$

Let us now consider the cases of Steel-208 and CFRP-210 series (Fig. 7). Although, the plates of both the series
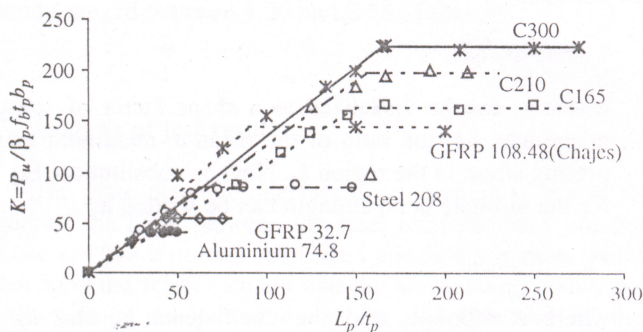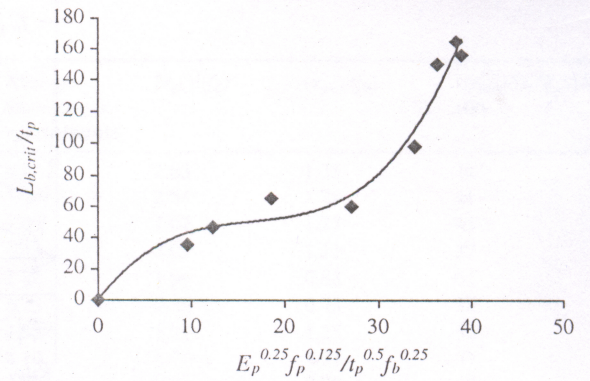

Fig. 8. $(L_{b,crit}/t_p)_{test}$ versus $(E_p^{0.25} f_p^{0.125}/t_p^{0.5} f_b^{0.25})$.

have similar elastic moduli (E_p), the value of $L_{b,crit}/t_p$ is higher in the case of CFRP-210 which has higher ultimate tensile strength than Steel-208. Similarly, the glass FRP [6] has a higher $L_{b,crit}/t_p$ value than that of Steel-208. Therefore, it can be said that E_p and f_p affect the ratio $L_{b,crit}/t_p$, in addition to the thickness of the plate and the tensile strength of the interface. Hence, to determine the ultimate bond strength (P_b) of plate, the two important factors are, K_{crit} and $L_{b,crit}$ that can be deduced as discussed below.

5.1. Expression for $L_{b,crit}/t_p$

The major parameters that affect the magnitude of $L_{b,crit}/t_p$ are the modulus of elasticity of plate E_p, thickness of plate t_p, splitting tensile strength of concrete f_b (taken as the tensile strength of the interface) and tensile strength of plate f_p. The regression of the test data of Table 2 (six series of present study) and test results [4,6,9] as depicted in Fig. 8, shows that the $L_{b,crit}/t_p$ is a function (a polynomial of degree three) of x in the form of

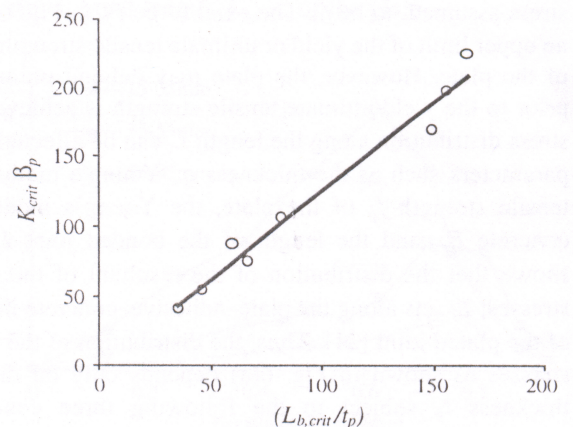$$L_{b,crit}/t_p = 0.0089x^3 - 0.439x^2 + 7.8645x, \tag{9a}$$

Fig. 7. Idealized K versus L_p/t_p.

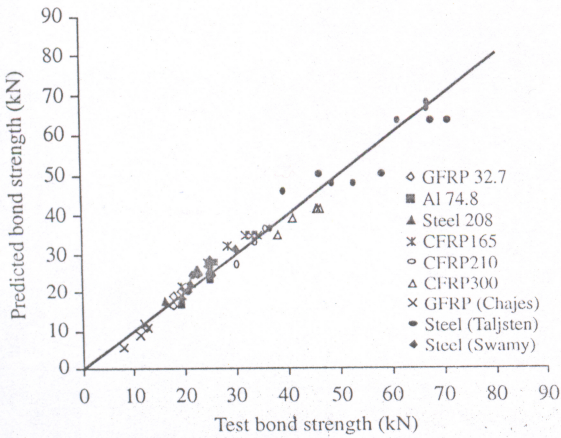Fig. 9. $K_{crit}\beta_{p\text{ (theory)}}$ versus $L_{b,crit}/t_{p\text{(theory)}}$ relationship.

Fig. 10. Test versus predicted bond strength.

where x is a non-dimensional parameter, and is given as

$$x = \frac{E_p^{0.25} f_p^{0.125}}{t_p^{0.5} f_b^{0.25}} \qquad (9b)$$

5.2. Expression for K_{crit}

The various values of K_{crit}, β_p and $L_{b,crit}/t_p$ obtained from Eqs. (8) and (9) for different types of plates are plotted in Fig. 9 and a best fit curve was drawn to obtain the relationship between K_{crit}, and $L_{b,crit}/t_p$

$$K_{crit} = 1.277 \frac{(L_{b,crit}/t_p)}{\beta_p} \qquad (10)$$

5.3. Expression for P_b

Substituting the expressions for $L_{b,crit}/t_p$ from Eq. (9a), K_{crit} from Eq. (10) and K from Eqs. (8), in (6) for bond strength (P_b), we get

$$P_b = \frac{K_{crit}\beta_p \left(\frac{L_b}{t_p}\right)}{\left(\frac{L_{b,crit}}{t_p}\right)} f_b t_p b_p, \quad \text{if } L_b/t_p < L_{b,crit}/t_p. \qquad (11a)$$

$$K_{crit}\beta_p f_b t_p b_p, \quad \text{if } L_b/t_p \geq L_{b,crit}/t_p. \qquad (11b)$$

P_b is always $\leq A_p f_p$, where $f_p =$ ultimate strength in case of linear elastic plates like FRP and yield strength in case of metallic plates.

The tests versus predicted ultimate bond strength results as obtained from Eq. (11) for the ultimate bond strength from the present study (Table 2) and the test results from the literature [4,6,9] are shown in Fig. 10, which shows a very narrow band for the results of 57 tests. The ratio of the predicted to the observed ultimate bond strengths ($P_{b \text{ theory}}/P_{b \text{ test}}$) has a mean value of 1.000 with a corresponding standard deviation of 0.091 and $R^2 = 1.00$. This can be considered that the relationship has very good correlation with low scatter despite the wide range of test results used

for calibration of the model. It is worth noting that the above models are valid for plate thickness more than 1 mm and within a wide range of geometric and material properties.

6. Conclusions

The direct single shear tests have shown that the debonding in reinforced concrete prisms, retrofitted with bonded steel, aluminum or FRP plate is always caused due to the initiation of the cracks in the vicinity of the most stressed end. The tensile strength of the plate has an effect on both the ultimate bond strength and critical bond length as determined from the tests. These critical parameters are found to depend on elastic modulus, tensile strength, width, and thickness, of the plate, as well as tensile strength of concrete and width factor. The design guidelines developed in this study are capable of predicting the ultimate bond strength (P_b) of beams bonded with metallic and non metallic plate with very good accuracy, and the model is validated with large number of test results.

References

[1] Oehlers DJ. Development of design rules for retrofitting by adhesive bonding or bolting either FRP or steel plates to RC beams in bridges and buildings. Proceedings of the ACUN-2, International Composite Conference 14–18 (2), University of New South Wales, Sydney, Australia;, 2000; 1.1, p. 110–9.

[2] Ali MSM, Oehlers DJ, Bradford MA. Shear peeling of steel plates adhesively bonded to the sides of reinforced concrete beams. Proc Instn Civil Eng Struct Bldg 2000;249–59.

[3] Ranisch EH, Rostasy FS. Bonded steel plates for reduction of fatigue stresses of coupled tendons in multi span bridges. In: Sasse HR, editor. Adhesion Between Polymers and Concrete. Paris: RILEM; 1986. p. 561–70.

[4] Swamy RN, Jones R, Sharif A. Shear adhesion properties of epoxy resin adhesives. Proceedings of International Symposium on Adhesion between Polymers and Concrete, Chapman and Hall, London, p. 741–755.

[5] Triantafillou TC, Plevris N. Strengthening of RC beams with epoxy-bonded fibre composite materials. Mat Struct, Paris 1992;25:201–11.

[6] Chajes MF, Januszka TF, Mertz DR, Thomson Jr. TA, Finch Jr, W W. Shear strengthening of reinforced concrete beams using externally applied composite fabrics. ACI Struct J 1996;5-6:295–303.

[7] Varastehpour H, Hamelin P. Analysis and study of failure mechanism of RC beams strengthened with FRP plates. 2nd Int Conf Adv Compos Mater Bridges Struct 1996;527–36.

[8] Arduini M, Nanni A. Behaviour of precracked RC beams strengthened with carbon FRP sheets. J Compos Constr 1997;1(2):63–70.

[9] Taljsten B. Defining anchorage lengths of steel and CFRP plates bonded to concrete. Int J Adhes Adhes 1997;17(4):319–27.

[10] Horiguchi T, Saeki N. Effect of test methods and quality of concrete on bond strength of FRP sheet. Non-Metallic (FRP) Reinforcement of Concrete Structures. Proc Third Int Symp 1997;1:265–70.

[11] Maeda T, Asano Y, Sato Y, Ueda T, Kakuta YA. Study on bond mechanism of carbon fibre sheet. Non-metallic (FRP) reinforcement of concrete structures. Proc Third Int Symp 1997;1:279–86.

[12] Bizindavyi L, Neale KW. Transfer lengths and bond strengths for composites bonded to concrete. J Compos Constr ASCE 1999;3(4):153–60.

[13] Malek AM, Saadatmanesh H, Ehsani MR. Prediction of failure load of RC beams strengthened with FRP plate due to stress concentration at the end of the plate. ACI Struct J 1998;95(1):142–52.

[14] Nakaba K, Kanakubo T, Yoshizawa T, Yoshizawa H. Bond behaviour between fibre-reinforced polymer laminates and concrete. ACI Struct J 2001;98(3):359–67.

[15] Sebastian WM. Significance of midspan debonding failure in FRP-plated beams. J Struct Eng 2001;127(7):792–8.

[16] Teng JG, Chen JF, Smith ST, Lam L. RC Structures Strengthened with FRP Composites. Hongkong, Chaina: The Hongkong Polytechnic University; 2000.

[17] Smith ST, Teng JG, Chen JF. Debonding in FRP plated RC beams induced by intermediate cracking. Proc ACUN-3 Int Conf: Technol Convergence Compos Applic, Sydney, Australia 2001;67–72.

[18] Hamoush SA, Ahmad SH. Debonding of Steel Plate-Strengthened Concrete Beams. J Struct Eng 1990;116(2):356–71.

[19] Jones R, Swamy RN, Charif A. Plate separation and anchorage of reinforced concrete beams strengthened by epoxy bonded steel plates. Struct Eng 1988;66(5):85–94.

[20] Roberts TM. Approximate analysis of shear and normal stress concentrations in the adhesive layer of plated R.C. beams. Struct Eng 1989;67(12/20):229–33.

[21] Oehlers DJ, Moran JP. Premature failure of externally plated reinforced concrete beams. J Struct Eng ASCE 1990;116(4):978–95.

[22] Oehlers DJ. Reinforced concrete beams with plates glued to their soffits. J Struct Eng ASCE 1992;118(8):2033–8.

[23] Sharif A, Al-Sulaimani GJ, Basunbul IA, Baluch MH, Ghaleb BN. Strengthening of initially loaded reinforced concrete beams using FRP plates. ACI Struct J 1994;91(3–4):160–8.

[24] Zirba YN, Baluch MH, Basunbul AM, Azad AK, Al-Sulaimani GJ, Sharif A. Combined experimental-numerical approach to characterization of steel glue-concrete interface. Mat Struct 1995;518–25.

[25] Quantrill RJ, Hollaway LC, Thorne AM. Experimental and analytical investigation of FRP strengthened beam response Part-I. Mag Conc Research 1996;48(177):331–42.

[26] Chajes MF, Januszka TF, Mertz DR, Thomson JrTA, Finch Jr, Bond WW. Bond and force transfer of composite materials plates bonded to concrete. ACI Struct J 1995;93(2):295–303.

[27] Neubauer U, Rostasy FS. Design aspects of concrete structures strengthened with externally bonded CFRP-plates. In: Proc 7th Int Conf Struct Faults Repair. Edinburgh: ECS Publications; 1997. p. 109–18.

[28] Breson, J. Nouvelle researches et applications concernant Putilisation des collages dans les structures. Beton plaque.1971. Annales de l'Institut Technique due Natiment et des Travaux Publics, Suppl. No. 278, Paris, 1971, p. 23–54.

[29] Barnes RA. Strengthening reinforced concrete beams in shear by the use of externally bonded steel plates. PhD thesis, Cranfield University (Yoyal Military College of Science); 2000.

[30] Chen JF, Teng JG. Anchorage strength models for FRP and steel plates bonded to concrete. J Struct Eng 2001;7:784–91.

[31] American Concrete Institute (ACI). Building code requirements for reinforced concrete. ACI 318-1989, Detroit.